Journal of Imaging Science and Technology® 56(4): 040501-1–040501-10, 2012.

Water-Based Carbon-Coated Copper Nanoparticle Fluid—Formation of Conductive Layers at Low Temperature by Spin Coating and Inkjet Deposition

K. Eiroma, J. Forsman, E.-L. Hult, A. Auvinen, T. Sipiläinen-Malm, A. Alastalo, U. Tapper, J. Leppäniemi, P. Mattila, and J. Lyyränen
VTT Technical Research Centre of Finland, FI-02150 Espoo, Finland
E-mail: kim.eiroma@vtt.fi

J. Sarlin
VTT Technical Research Centre of Finland, FI-33101 Tampere, Finland

J. Jokiniemi
VTT Technical Research Centre of Finland, FI-02150 Espoo, Finland University of Eastern Finland, Department of Environmental Science, FI-70211 Kuopio, Finland

S. Mössmer
BYK-Chemie GmbH, DE-46483 Wesel, Germany

Abstract. *A conductive inkjettable fluid was formulated based on carbon-coated copper nanoparticles. The copper particles were produced by vapor-phase reduction of copper chloride and coated in situ with carbon. The average particle size was 44–88 nm depending on the chosen production parameters. The optimized fluid was a water/ethylene glycol monobutyl ether/n-propanol mixture with 25 wt% nanoparticles, stabilized by a polymeric dispersing agent. A conductivity of 6.4 S/m was obtained with a single deposited layer without sintering or high-temperature annealing. The materials are interesting for several applications such as antistatic coatings, resistors, and sensors. © 2012 Society for Imaging Science and Technology.*

[DOI: 10.2352/J.ImagingSci.Technol.2012.56.4.040501]

INTRODUCTION

There is currently a strong drive towards the development of low-cost conductive metallic nanoparticle-based fluids for printed electrically functional devices.[1] Significant interest has lately been directed towards replacing silver and gold with copper due to its low price. The specific challenge in processing of copper is its tendency to oxidize in ambient conditions. Several ways of protecting copper nanoparticles from oxidation have been reported.[2] High conductivities for inkjet-deposited copper patterns have so far been obtained for surfactant and polymer-stabilized copper nanoparticles as well as copper nanoparticles encapsulated with a secondary metal, such as silver. In most cases, high-temperature sintering and removal of the stabilizing layer in an oxygen-free environment has been required to achieve conductivities in the 10^6–10^7 S/m range (∼10–20% of bulk copper).[3–5] Recently, low-temperature photonic curing in air has made advances, and conductivities one third of that of bulk copper have been demonstrated for inkjet-printed copper nanoparticle fluids.[6] An alternative approach for stabilizing copper nanoparticles has been presented by Luechinger et al.,[7] where the flame spray technique was used for particle production and a conductivity of 1.5 S/cm for a 10-layer inkjet-printed line pattern was attained by drying at 120°C in air. The particles were coated with a 3 nm thick graphene layer, which rendered them air stable. Other methods have been used to coat copper nanoparticles with carbon, including pyrolysis, which was used by Schaper et al.,[8] yielding particles with a copper core diameter of 50 nm and carbon shell thickness of 60–80 nm. Recently, Wang et al.[9] produced air-stable multi-layer graphene-encapsulated copper nanoparticles by metal–organic chemical vapor deposition and suggested their use in conductive inkjet fluid formulations. However, to the best of our knowledge, demonstrations of conductive layers from inkjet-printed or by other means deposited carbon-coated copper nanoparticle fluid dispersions are limited to the work by Luechinger et al.[7]

Low resistivity approaching that of bulk metals is desired for most printed electronics applications such as antennas, optoelectronic devices, passive and active components, and device interconnects. However, in antistatic coatings for, for example, packaging, higher surface resistivities in the range 10^4–10^{11} $\Omega/\square$ are typical.[10] The material could also be applied for resistors and sensors.[11] Although, in principle, removal of the protective carbon layer through various types of post-processing could be possible in order to achieve actual copper-to-copper contact and subsequent sintering and higher conductivity, the current application potential of these materials is in devices that require low conductivity.

Typically, high molecular weight polymeric stabilizing ligands are used for dispersing nanoparticles into a fluid for solution processing. The amount and type of the electrically insulating stabilizing agent determines the final obtainable

---

Received May 2, 2012; accepted for publication Sep. 19, 2012; published online Dec. 6, 2012.
1062-3701/2012/56(4)/040501/10/$20.00

Table I. Overview of particle production parameters. Flow is given at liters per minute at normal temperature an pressure (Nlpm).

Material	C_2H_4 concentration in reaction flow (mol%)	H_2O bubbling flow (Nlpm)	Number average particle diameter (nm)
Cu+C	0.05	0	88
Cu+C	0.92	0	44
Cu+CNT	0.92	0.5	44–66

conductivity level when processing the deposited layer at low temperatures, since it is not completely removed at these temperatures. In addition, conductivity relies on achieving an optimum degree of interparticle contact for charge transport.

The fluid solvent composition can affect the layer morphology and particle packing through its effect on the drying behavior of the deposited layer. It is well known that the migration of solute during drying of a single-solvent particle-laden fluid towards the perimeter of the deposited fluid layer on a smooth wetting solid surface[12] leads to an inhomogeneous distribution of the particles in the dried layer. The formation of these "coffee ring" deposits is caused by an outward convective flow which attempts to replenish the solvent that is evaporated at a higher rate at the edge (pinned contact line) of the deposited fluid than at the center.[13] A Marangoni flow can be induced to counteract the outward convective flow by addition of a high boiling point/low surface tension solvent into a low boiling point/high surface tension single-solvent (e.g. water-based) system.[14,15]

In this study, we have produced a fluid that is very low in cost and suitable in the aforementioned low-conductivity applications. The aim was to produce a low-conductivity layer with minimal processing steps at low temperature, making the process compatible with substrates such as paper, cardboard, and plastic films having a low glass transition temperature (T_g). The air-stable carbon-coated copper particles for the fluid are produced via the aerosol synthesis route, which is characterized by high mass concentration and yield.[16] The process is continuous and thereby scalable towards economic high-volume production. The effect of dispersing agent and solvent composition on the dispersion stability of the water-based fluid and the electrical properties of deposited layers as well as on the fluid's inkjettability is investigated. We demonstrate conductivity obtained by a single deposited layer of the stable fluid dispersion having 25 wt% nanoparticles.

MATERIALS AND METHODS

Particle production

Carbon-coated copper nanoparticles were produced by hydrogen reduction of metal chloride precursors at high temperature (950°C). The technique was developed previously for the production of metal nanoparticles.[16] A powder feeder (Lambda Doser) was used to feed copper chloride powder (Sigma-Aldrich, 97% purity) to a bed of porous alumina pellets (SASOL) that was inside the quartz reactor. This evaporation zone was heated to 750–800°C and the copper chloride precursor was evaporated in a nitrogen flow. The flow continued to the reaction zone, where it was mixed with hydrogen (13.8 mol%), ethene (0.05 and 0.92 mol%) and H_2O vapor (500 ppm). The copper chloride reacts with hydrogen producing copper and hydrogen chloride. Ethene reacts partly producing a carbon coating and multi-walled carbon nanotubes (MWCNTs) on the copper particles. The particles produced as above are referred to as Cu+CNT. As a reference, carbon-coated particles without MWCNTs (Cu+C) were produced without the H_2O vapor but otherwise as above (Table I).

The flow coming out of the reactor was diluted and cooled with nitrogen with a dilution ratio of 7.7 to prevent further agglomeration and sintering of the particles. Unless otherwise specified, all concentrations are reported in this once-diluted flow at NTP. The produced powder was then collected in a PTFE filter bag. Fourier transform infrared (FTIR) spectroscopy (Gasmet DX4000) was applied to measure the concentrations of HCl in order to monitor the particle production rate. FTIR spectroscopy also measured the concentration of water vapor, and of gas impurities CO and CO_2, as well as the gaseous degradation products of ethene. HCl was removed downstream of the filter from the exhaust flow using two tanks filled with NaOH–water solution before the flow was directed to an exhaust duct. 90–95 wt% of the produced particle mass as calculated from FTIR data could be retrieved from the collection filters.

Gravimetric analysis of particle mass concentration was conducted by taking samples with 47 mm analysis filters (Millipore 0.2 μm FG Fluoropore, flow rate 0.38 Nlpm) for 1 min. These samples were also used for transmission electron microscopy (FE-TEM, Philips CM-200 FEG equipped with an EDS analyzer) to determine the particle size distribution from the images. The number average diameter (NAD), standard deviation (SD), and specific surface area (SSA TEM) were determined from the micrographs of 150–500 particles.

The structure of the particles was studied with X-ray diffraction (XRD, Philips X'pert MPD X-ray diffractometer) and composition with X-ray fluorescence (XRF, Philips PW2404 X-ray spectrometer with SemiQ). The oxidation behavior of the particles was analyzed thermogravimetrically (TGA, Mettler TGA 851e). The sample was heated at a rate of 5°C/min in a 50 ml/min air flow from 25 to 500°C. Assuming full oxidation to CuO, the analysis was also used to estimate the carbon content of the carbon-coated particles. The SSA

Table II. Average molecular weights (Mw, Mn) and polydispersities (Mw/Mn) of dispersing agents.

Dispersing agent	Name	Mw (Daltons)	Mn (Daltons)	Mw/Mn
Disperbyk-190	[Disp_1]	29,400	10,200	2.88
Disperbyk-198	[Disp_2]	37,600	16,100	2.35
Disperbyk-2012	[Disp_3]	31,300	13,700	2.28

Table III. Viscosity, surface tension, and boiling point of solvents.

	Viscosity, η (mPa s at 20°C)	Surface tension, γ (mN/m)	Boiling point (°C)
DIW	1.0	72	100
EGBE	3.3	27	171
EGME	2.0	33	125
n-propanol	2.2	24	97

was measured directly using the BET method (ASAP2020, Micromeritics Instruments Co.) and compared with the SSA calculated from TEM images.

The particle concentration and size distribution of the Cu+CNT particles were also measured directly from the gas phase. Because the number concentration of the particles is very high, a sample flow from the once-diluted reaction flow entered a multi-stage dilution system. Depending on the rate of the CuCl feed, the dilution system consisted of a porous tube diluter (PRD[17]) connected in series with either two or three ejector-type diluters (EDs[18]). The total dilution ratios (DRs) were 239 (PRD + 2 EDs) and 2453 (PRD + 3 EDs). The dilution gas for all diluters was nitrogen.

A scanning mobility particle sizer (SMPS) measured the number concentration and number size distribution of the particles after the described multi-stage dilution. An SMPS consists of a differential mobility analyzer (DMA, TSI model 3080 with tube model 3081) and a condensation particle counter (CPC, TSI model 3775). Prior to entering the DMA, large particles (>0.6 μm; depending on the setup) are removed by a pre-impactor mounted on the DMA inlet. The size distribution is obtained by varying the DMA voltage and calculating the concentration of particles in each electrical mobility class by the CPC.[19–21] The measurement range in the setup used was 10–420 nm. The SMPS data directly observes the count median diameter (CMD) and geometric standard deviation (GSD). For comparison with the size distribution determined from TEM images, the number average diameter and sample standard deviation were also calculated from the SMPS data.

Fluid preparation

The dispersing capability of the nanoparticles was evaluated using three high molecular weight dispersing agents intended for water-based carbon black pigment dispersions by BYK Chemie Gmbh, DISPERBYK-190, DISPERBYK-198, and DISPERBYK-2012, hereafter denoted [Disp_1], [Disp_2], and [Disp_3], respectively. The molecular weights and polydispersities, obtained by size exclusion chromatography, are shown in Table II. The molecular weight and structure of the dispersing agents are similar, the main differences being the nature of the backbone and the functional groups. The backbone of [Disp_1] and [Disp_3] is mainly composed of vinylic monomers, whereas the backbone of [Disp_2] has a different structure (undisclosed by the supplier). The pigment affinic groups of all dispersing agents contain hydrophobic groups for hydrophobic interaction in a water-based system. In addition, [Disp_1] contains acidic groups, [Disp_2] contains basic (aminic) groups, and [Disp_3] contains special ionic groups.

De-ionized water (DIW) was used as the main solvent. Ethylene glycol monomethyl ether (EGME) (Sigma-Aldrich), ethylene glycol monobutyl ether (EGBE) (Merck), and n-propanol (Honeywell Riedel-de Haen) were used as co-solvents for improving the fluid-jetting and layer-forming properties through their viscosity, surface tension, and volatility (Table III).

The nanoparticles were mixed with the dispersing agents, co-solvents, and DIW, and the suspension was sonicated for 10 min in an ice bath at an intensity of 30% (1.0 cycle) using a UP400S ultrasonic processor (Hielscher Ultrasonics). Thereafter, the suspension was left to settle for an hour followed by decanting. Prior to spin coating or printing, the suspension was sonicated in an ultrasonic bath for 10 min.

The rheological properties of the fluid were measured using a Physica MCR 301 rheometer (Anton Paar). The fluid sample was placed in the space between a plate and a cone with an angle of 2° and a radius of 50 mm. The measurement was performed at a shear rate ranging from 0.2 s^{-1} to 300 s^{-1} at 23°C. The fluid surface tension was measured using an EZ-Pi tensiometer (Kibron). Dispersion stability at room temperature was evaluated qualitatively by visually determining the degree of particle sedimentation and phase separation at regular intervals.

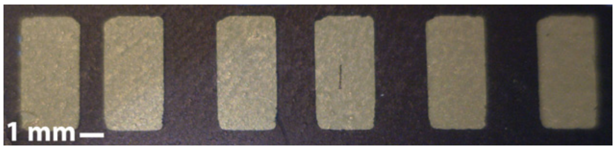

Figure 1. Gold electrode pairs of 1.0, 1.5, and 2.0 mm inter-electrode distances grown by thermal vacuum evaporation on a dried Cu+CNT layer deposited by spin coating.

Layer deposition

Spin coating of the nanoparticle dispersions was carried out using an EC101D series spin coater (Headway Research) at 1000 rpm for 1 min. Inkjet printing was carried out with a DMP-2831 laboratory-scale piezoelectric drop-on-demand printer (Fujifilm Dimatix). The printer utilizes printhead cartridges with 16 nozzles arranged linearly at a pitch of 254 μm. Cartridges generating a nominal drop volume of 10 pL were used. Printing was performed at a jetting frequency of 1 kHz. Printing of solid fill layers for electrical characterization as well as single-pixel-width lines for studying layer morphology was carried out at 20 μm inter-drop spacing (1270 dpi).

Layers were deposited on microscopic glass slides (Thermo Scientific). The glass substrates were cleaned by immersion in acetone followed by immersion in isopropanol, both under ultrasonication for 10 min, and drying under nitrogen flow. A single layer for both inkjet printing and spin coating was applied. The spin-coated and printed layers were immediately dried on a hot plate for 60–90 s at 60°C and then transferred to an oven for drying at 105°C in air for 1 h.

For electrical conductance characterization, gold electrode pairs having a thickness (D) of 100 nm, inter-electrode distances (channel/gap lengths, L) of 0.8, 1.0, 1.5, and 2.0 mm and electrode (channel) widths (W) of 10 and 40 mm, were grown by thermal vacuum evaporation on the deposited copper–carbon layers (Figure 1). After oven drying, and prior to electrical characterization, samples were stored in a nitrogen glove box.

The topographies of the dried spin-coated and printed layers were characterized by optical microscopy (BX60, Olympus), stylus profilometry (Dektak 150, Bruker AXS), and scanning electron microscopy (SEM) imaging (LEO DSM 982 FE-SEM and LEO Supra 35 FE-SEM). Electrical characterization of the dried copper–carbon layers was performed by 2-point probe resistance measurements using a digital multimeter (Agilent 34411A) from the thermal vacuum evaporated gold electrodes. The temperature–resistance dependence was measured using a setup consisting of a closed chamber precision controlled temperature ramping hot plate (Instec HCP622V) and a data acquisition/switch unit (Agilent 34970A) for on-line 2-point probing. The ohmic character of the deposited layers was verified by a digital sourcemeter (Keithley 2636) in the voltage range −10–10 V. The layer conductivity ($\sigma = LR^{-1}W^{-1}D^{-1}$) was calculated using measured values for resistance (R), electrode gap length (L) and width (W), and layer thickness (D).

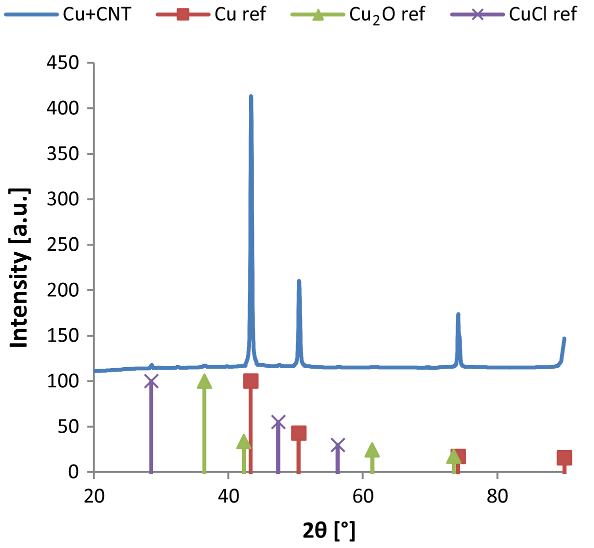

Figure 2. XRD measurement of Cu+CNT particles. The copper peaks are very clear and the contribution of Cu_2O and CuCl is just above the detection limit.

RESULTS AND DISCUSSION

Carbon-coated copper nanoparticle synthesis and characterization

The XRF analysis revealed that the Cu+C particles for ethene concentrations of 0.92 mol% consisted of 83–84 wt% copper and 15–16 wt% carbon. The main impurity was Cl with a maximum concentration of 0.8 wt%. Ni, Si, P, Co, and S constituted the remaining <0.1 wt%. These concentrations are consistent with XRD analysis; see Figure 2 for typical XRD data. Cu is the major contribution, with some CuO and Cu_2O present. For the Cu+CNT particles, the copper concentration was 90 wt% according to XRF. The concentration of carbon was 9 wt%, of chlorine 0.9 wt%, and of Si, S, and Co $<$ 0.2 wt%. This is consistent with XRD, which shows, in addition to clear cubic Cu peaks, minor CuCl and Cu_2O contributions. The particle properties are summarized in Table IV.

In TGA, the oxidation of copper depends on the carbon layer, as shown in Figure 3. For Cu+C particles with 0.05 mol% ethene in the reaction flow, the oxidation initiates at 155°C. For Cu+C particles with 0.92 mol% ethene, oxidation initiates at 101°C. This may be due to the better defined crystal structure of the carbon coating formed at the lower ethene concentration. With the higher ethene concentration, formation of the carbon coating was faster, and thus the crystal structure is likely to have more defects. The carbon mass fraction observed according to TGA is 11.1 wt% for Cu+C with 0.92 mol% ethene. Most likely some of the carbon formed carbon dioxide already during the oxidation of copper, and thus the final weight loss underestimates the carbon content of the sample. Therefore it is likely that the XRF-analyzed carbon content is closer to the actual carbon concentration.

A TEM micrograph of the Cu+CNT particles with an ethene concentration 0.92 mol% in the reaction flow is shown in Figure 5. According to FTIR spectroscopy, the mass

Table IV. Overview of particle properties for comparable Cu+C and Cu+CNT particles. The ethene concentration was 0.92 mol% in both cases.

	NAD (nm)	STDEV (nm)	SSA, BET (m^2/g)	SSA, TEM (m^2/g)	C, XRF (wt%)
Cu+CNT	66	27	14	7.9	9
Cu+C	64	27		7.8	15

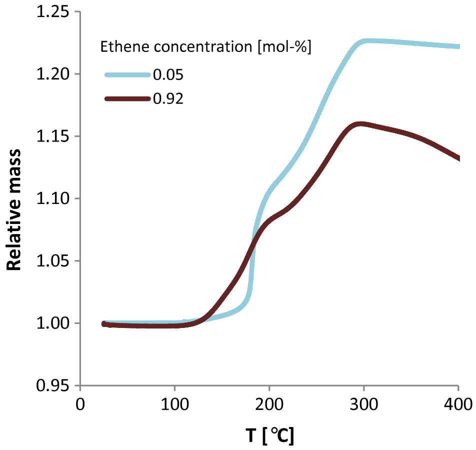

Figure 3. TGA curves for Cu+C particles produced with 0.05 and 0.92 mol% ethene. The burning of the carbon may occur at the same time as oxidation, which would underestimate the copper content for the high ethene concentration sample.

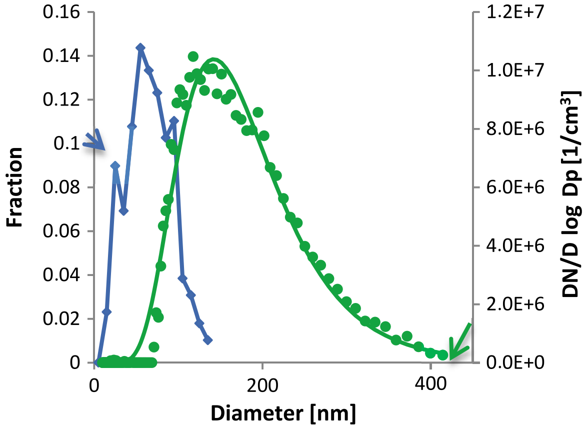

Figure 4. Size distribution of Cu+CNT nanoparticles as determined from TEM micrographs (left) and SMPS (right). The electrical mobility size measured by SMPS is significantly larger than the TEM number average diameter. The TEM diameter is the size of the Cu core, whereas the SMPS diameter also includes the tubular structures growing from the particles, making the diameter much larger. In addition, SMPS measures agglomerates, whereas the TEM distribution only describes primary particles.

concentration of copper in the reactor varied between 3 and 5 g/m^3 (NTP) during the production of the powders. The number average diameter (NAD) of the particles was 66 nm and the standard deviation 27 nm. The size distribution is illustrated in Figure 4. According to BET and TEM, the SSA of the powder was 14 m^2/g and 7.9 m^2/g, respectively. In BET analysis the SSA is higher, since MWCNT structures increase the surface area of the sample relative to the smooth surface and solid sphere assumption used in SSA calculations from the TEM images. In high-resolution TEM images, lattice lines with 0.34 nm spacing are observed (not visible in Fig. 5), indicating a graphene-like layered tubular structure.

The particle number concentration measured with SMPS for the Cu+CNT particles was 4.5×10^6 $1/cm^3$, with a CMD of 142 nm (Table V). The SMPS number size distribution is compared to the TEM number size distribution in Fig. 4. The smallest copper particles seen in the TEM distributions are also those that are mainly responsible for the MWCNT structures. The MWCNT structures increase the mobility diameter measured by SMPS but are not taken into account when the diameter of the copper particles is determined with TEM. In addition, the particles form agglomerates, seen in the SMPS size distribution as increased particle diameter.

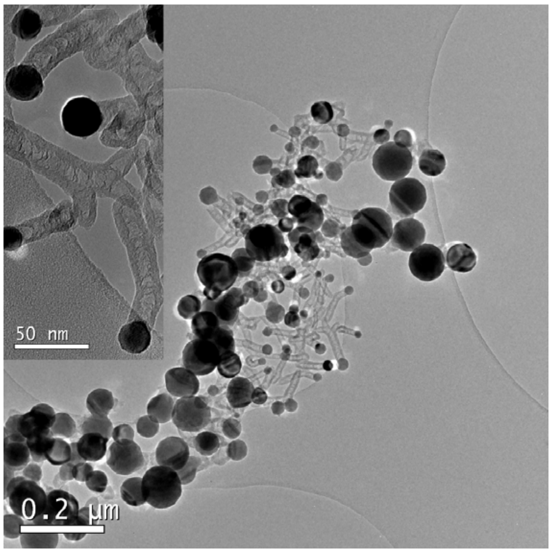

Figure 5. TEM image of Cu+CNT particles. The inset figure shows the MWCNT structures in more detail (scale bar: 50 nm). The copper particle size associated with CNT growth is less than 35 nm in diameter. The width of the MWCNT structures is about 20 nm.

Deposition of Cu+CNT fluid by spin coating

A fluid composition consisting of Cu+CNT particles (25 wt%), DIW (50 wt%) and n-propanol (25 wt%) was used for characterization of the effects of the dispersing agents. Spin coating was used as the deposition method. Due to the high volatility and low viscosity of its constituents, the fluid was assumed not to have sufficient inkjetting performance for obtaining repeatable layers for electrical characterization.

Table V. The size distribution characteristics from SMPS measurements and the corresponding mass concentration from the FTIR measurement.

Experiment	Mass concentration (FTIR) (g/m^3)	N_{tot} (DMA) (1/cm^3)	CMD (nm)	GSD	NAD (nm)	STD (nm)
Cu+CNT	3–5	4.5E+06	142	1.5	153	63

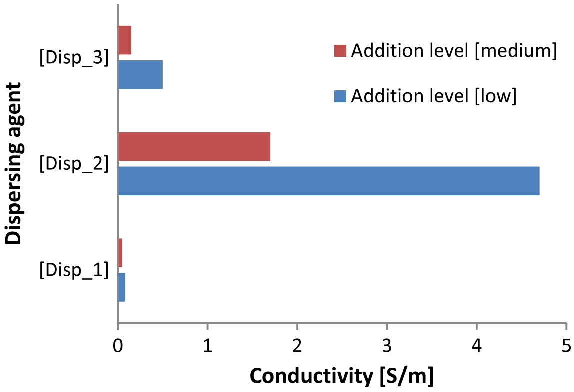

Figure 6. Effect of dispersing agent type and addition level on the conductivity of spin-coated and dried Cu+CNT fluid layer.

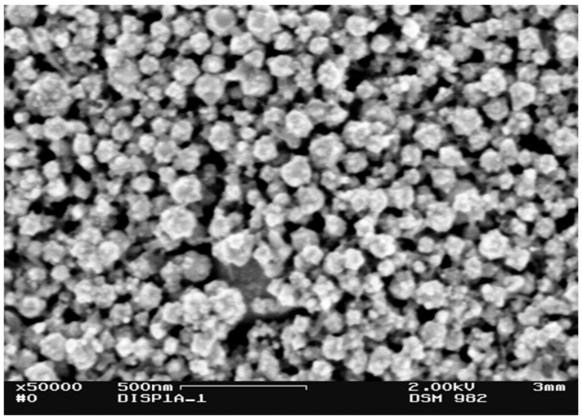

Figure 7. SEM image at 50,000× magnification of sample [Disp_2][low] exhibiting the highest conductivity.

Figure 6 shows the conductivity obtained from varying the addition level and type of dispersing agent. Addition level 8 wt% of dispersing agent on Cu+CNT particles is denoted as [low] and 16 wt% as [medium]. All dispersions except [Disp_1][low] appear stable for a period of 5 days, after which gradual phase separation and sedimentation of the particles is observed. The better dispersion stability provided by [Disp_2] and [Disp_3] compared to [Disp_1] may be explained by the basic pigment affinic groups and special ionic groups, respectively, interacting with the residual acidic groups (HCl) adsorbed on the Cu+CNT particle surfaces.

A higher conductivity is observed for addition level [low] for all dispersing agent types, most clearly for [Disp_2], which also provides the highest conductivity (4.7 S/m, ~ 7 orders of magnitude lower than the bulk Cu conductivity of 5.96×10^7 S/m). The linear current–voltage curves indicate ohmic resistance of the deposited layer and give resistances very close to the low-voltage 2-point multimeter results obtained.

Although results indicate substantial variation in the range 20–50%, it seems evident that, if the stabilizer to nanoparticle ratio is too high, the organic polymers will act as an insulator and prevent direct contact between the conductive particles.[22] The same dispersing agent to nanoparticle ratio for different dispersing agents results in different conductivities. The higher conductivities obtained by [Disp_2] may be due to the different (undisclosed) polymer backbone structure decomposing or fragmenting more easily compared to the backbone of [Disp_1] and [Disp_3] (mainly composed of vinylic monomers) during the drying treatment.

Figure 7 shows an SEM image at 50,000× magnification of sample [Disp_2][low] exhibiting the largest obtained conductivity, taken from the center region of the channel between the evaporated gold electrodes. The layer morphology and packing of the particles are, however, representative of all samples, suggesting that differences in conductivity are likely to arise from the degree of interparticle insulation provided by the non-conducting polymeric dispersing agents.

Preliminary jetting tests of composition [Disp_2][low] reveal unstable drop formation properties at a jetting frequency of 1 kHz, even when adjusting the nozzle driving voltage and waveform for optimized droplet pinch-off from the nozzle and merging of the trailing ligament (tail) with the main drop. Numerous studies, reviewed for example by Derby,[23] have shown that an increase in viscosity from the level of, for example, water (1 mPa s) to the range considered optimum for industrial piezoelectric drop-on-demand (piezo DOD) inkjet (typically around 10–20 mPa s), results in more stable satellite-free droplet generation when aiming for higher droplet velocities and jetting frequencies. Even though a viscosity measurement is not available for confirmation, the known viscosities of the fluid components (DIW, n-propanol) (Table III) suggest that the viscosity of the composition is considerably lower than the typical range for industrial piezo DOD inkjet and also the range suggested as optimum by the printer manufacturer. In addition, jetting latency is poor, most likely due to the absence of a fluid component with low volatility. It is well known that the latency of drop formation in a piezo DOD printhead is significantly increased by the addition of a high boiling point solvent.[24]

Table VI presents the Cu+CNT fluid compositions based on dispersing agent [Disp_2] at addition level [low], to which co-solvents EGBE and EGME have been added

Table VI. Fluid compositions with varying ratios of de-ionized water/n-propanol/co-solvent. 8 wt% of dispersing agent [Disp_2] was added relative to a particle loading of 25 wt%.

Composition	[A]	[B]	[C]
DIW (wt%)	50	50	25
n-propanol (wt%)	18.7	12.5	25
Co-solvent (EGME or EGBE) (wt%)	6.3	12.5	25

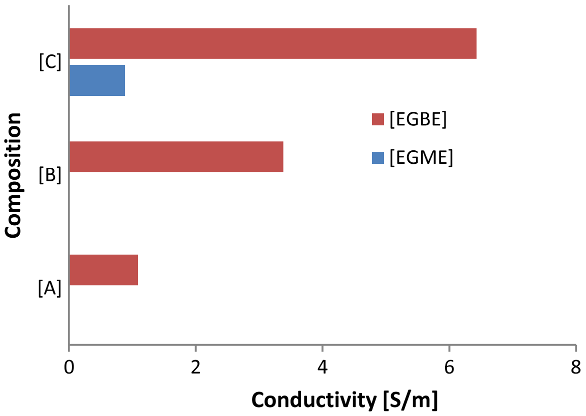

Figure 8. Conductivities of spin-coated and dried layers of Cu+CNT compositions [A], [B], and [C] with EGME and EGBE as co-solvent.

for adjusting the properties of the spin-coated formulation towards inkjetting capability, i.e., higher viscosity and lower volatility. The boiling points of both co-solvents are also not exceedingly high considering the targeted low-temperature (105°C) drying conditions.

Figure 8 presents the conductivities obtained for compositions [A], [B], and [C]. Spin coating was used as the deposition method in order to bypass the possible challenges of obtaining reproducible layers for electrical characterization by inkjet deposition. For compositions containing EGME as co-solvent, only composition [C] exhibits similar prolonged stability (>5 days) to the compositions containing EGBE as co-solvent. Therefore compositions [A][EGME] and [B][EGME] are not included in Fig. 8.

An increase in the ratio of EGBE to n-propanol and DIW has an increasing effect on layer conductivity, the maximum obtained conductivity being 6.4 S/m for composition [C][EGBE]. The conductivity for composition [Disp_2][low] in Fig. 6 is on the same level. Direct comparison of conductivity values is complicated by the fact that the compositions were prepared from different batches of Cu+CNT particles. A reference composition without EGBE was not prepared from the same batch. Current–voltage curves indicate ohmic resistance for the deposited layers. Overall, a 14–20% variation in measured conductivities is observed. For composition [C], using EGBE as co-solvent results in significantly higher conductivity than when using EGME as co-solvent.

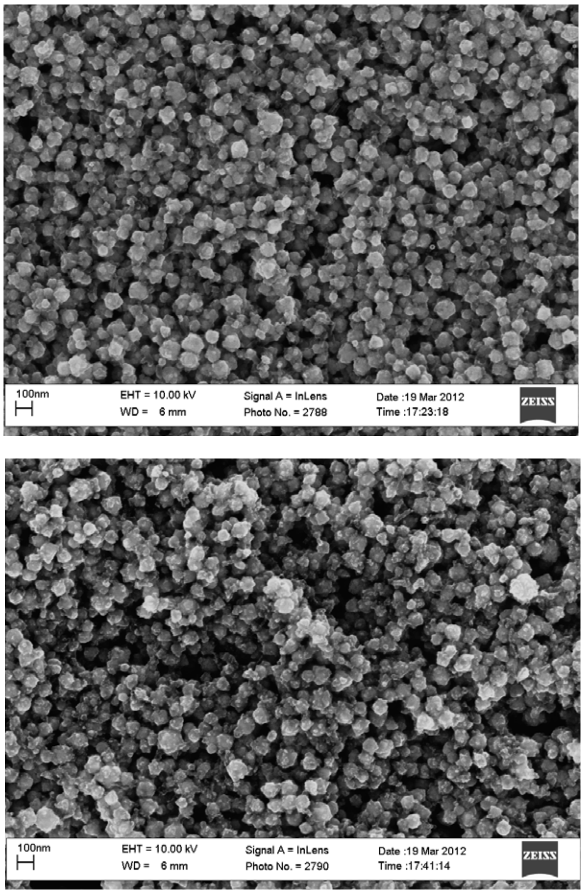

Figure 9. SEM images at 100,000× magnification of spin-coated layers of Cu+CNT compositions [C][EGME] (top) and [C][EGBE] (bottom).

It is suggested that the higher conductivity of [C][EGBE] compared to [C][EGME] is due to the differences in boiling point and surface tension of the co-solvents, which affect the particle distribution during drying of the deposited layer. As the boiling point of EGME (125°C) is relatively close to that of the main solvent, water (100°C), a sufficiently large concentration and surface tension gradient will likely not form to induce an inward Marangoni flow for composition [C][EGME], which is expected to behave similarly to a single-solvent fluid where the outward convective flow dominates.[15] The boiling point of EGBE (171°C), however, is sufficiently high to create a concentration gradient and resulting surface tension gradient for creation of an inward Marangoni flow. The surface tension for EGBE (27 mN/m) is also slightly lower than for EGME (33 mN/m), which contributes to the surface tension gradient as well.

SEM images in Figure 9 show more agglomeration of particles in the spin-coated layer for composition [C][EGBE] than for [C][EGME]. This may also be an indication of flows induced within the drying layer as a result of the discussed mixed solvent composition, which has a favorable effect on interparticle organization and conductivity.

In the context of inkjet-deposited particle-laden droplets and beads with pinned contact lines, the above-described convective flow and Marangoni flow induced morphologies have been observed very clearly.[14,15] For spin-coated colloidal fluids, the same compositional gradient driven flows have been observed to affect the layer morphology and the creation

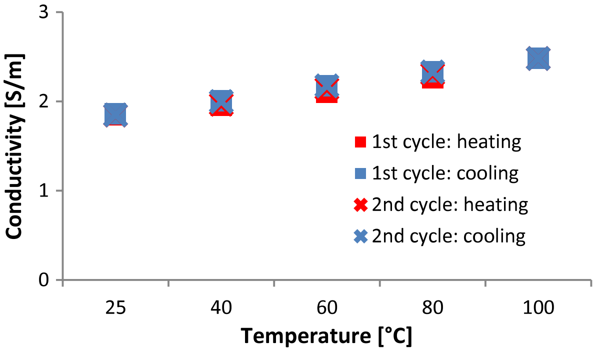

Figure 10. Conductivity of [C][EGBE] as a function of temperature. Two heating cycles from room temperature to 100°C are shown.

of defects, such as striations (layer thickness variation) in the dried film.[25,26] The compositional gradient is essentially occurring in the thickness direction of the drying film. Therefore it is suggested that convective and compositional gradient driven flows influence the morphology of the spin-coated Cu+CNT particle layer, and are responsible for the differences observed in the conductivity values in Fig. 8.

The conductivity of a spin-coated layer of composition [C][EGBE] is presented in Figure 10 as a function of temperature. A relatively linear increase of 0.16 S m^{-1} C^{-1} is observed from room temperature up to 100°C. Two consecutive heating/cooling cycles show that the hysteresis effect is low. The *c*-axis conductivity of highly oriented pyrolytic graphite (HOPG) has been measured to be 0.1 S/m at room temperature ($T = 300$ K). Unlike the case of metals, the *c*-axis conductivity of HOPG also demonstrates insulating-like behavior for $T > 50$ K, increasing linearly with temperature.[27] Our result indicates that the layer of graphitic carbon on the copper particles primarily defines the conductivity of the deposited particle layer.

Jetting tests using composition [C][EGBE], having the highest concentration of the highest viscosity and lowest volatility component (EGBE, 3.3 mPa s/171°C), show an improvement towards more stable (more controlled tail pinch-off and merge, fewer satellite droplets) and more sustainable jetting performance compared to composition [Disp_2][low] (in Fig. 6) without co-solvent addition. Characterization of drop formation of the fluid suggests that relatively stable jetting at a drop velocity of $\sim$5 m/s is attained at jetting frequencies up to 5 kHz. The drop formation process is characterized by a breaking up of the trailing ligament into 1–2 satellite droplets which merge with the main drop at a distance of 1 mm from the nozzle exit. The measured fluid viscosity is relatively stable at $\sim$8 mPa s at shear rates in the 100–300 s^{-1} range (data not shown). Even though this result gives an indication of the behavior of the fluid at higher shear rates, higher-frequency rheological measurements are suggested to more accurately characterize a fluid's jetting behavior in the kilohertz range.[28] The viscosity is just below the typical piezo DOD range (10–20 mPa s) and the recommended range for the DMP-2831 printer (10–12 mPa s), which can explain the suboptimal jetting performance. The viscosity could be increased by substituting EGBE (viscosity 3.3 mPa s @ 20°C) with a higher viscosity co-solvent that has a similar boiling point, such as ethylene glycol (viscosity 18 mPa s @ 20°C, boiling point 197°C). The surface tension of 26.7 mN/m is slightly below the typical optimum range of 30–40 mN/m, and may also be the cause of unstable tail pinch-off and break-up.[29]

Table VII. Cu+C fluid compositions with varying ratios of de-ionized water/n-propanol/EGBE. 8 wt% of dispersing agent [Disp_2] was added relative to a particle loading of 25 wt%.

Composition	[C]	[K]	[L]
DIW (wt%)	25	22	19
n-propanol (wt%)	25	19	15
EGBE (wt%)	25	34	41

Deposition of Cu+C fluid by spin coating and inkjet

The effect of co-solvent concentration on the electrical performance of spin-coated and inkjet-deposited layers is further investigated using compositions [C] (as reference), [K], and [L] (Table VII). For these compositions, Cu+C particles were used because sufficient quantities of synthesized Cu+CNT particles were not available for preparation of the required volume of fluid for inkjet deposition. For compositions [C], [K], and [L], the ratio of high boiling point to low boiling point solvents increases, which is accompanied by a conductivity increase, as observed in Figure 11, similarly to the results in Fig. 8.

A conductivity of 0.34 S/m, an order of magnitude lower than for the Cu+CNT-based composition (Fig. 8), is obtained for a spin-coated layer of composition [C][EGBE] on glass. The variation is in the range 16–26%. Linear current–voltage curves indicate ohmic resistance of the deposited layers. The conductivity difference to the Cu+CNT fluid can be explained by the MWCNTs forming bridges between particles that would otherwise not have established contact for charge transport. A generally poorer stability of the Cu+C-based dispersions compared to the Cu+CNT dispersions is observed as well, which can possibly be explained by the more effective steric stabilization provided by the CNTs.

The conductivities obtained for inkjet-deposited layers are lower than the values obtained for spin-coated layers for compositions [C] and [K]. However, for composition [L] with the highest high to low boiling point solvent ratio, the inkjet-deposited layers provide a similar or slightly higher conductivity (0.88 S/m) than the spin-coated layers (0.75 S/m). Jeong et al.[15] found that an optimized mixed solvent composition for controlling the flow of solvent during drying was responsible for the similar conductivity level ($\sim 10^7$ S/m) obtained for inkjet-deposited and spin-coated layers of a copper nanoparticle fluid, suggesting that the spin-coated layer dried uniformly and produced films of optimum morphology whereas the inkjet-deposited layer formation was to a larger extent subject to the hydrodynamic

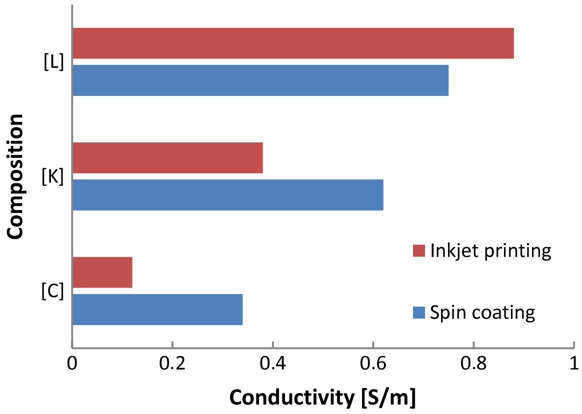

Figure 11. Conductivities of inkjet-printed and spin-coated and dried layers of Cu+C compositions [C], [K], and [L].

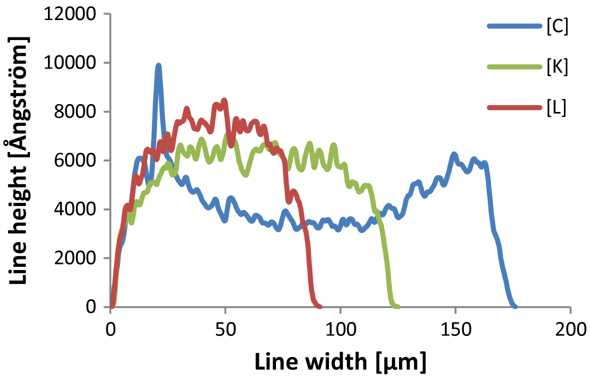

Figure 12. Line profile scans of inkjet-deposited single-droplet-wide lines of Cu+C fluid compositions [C], [K], and [L].

flows discussed previously. In the results presented in this article, however, the effect of solvent composition on conductivity through layer uniformity seems evident for spin coating as well. Similarly to the work of Jones and Smith,[15] at a certain solvent composition ratio the layer uniformity of inkjet-deposited and spin-coated layers seems to be comparable, at least as observed through obtained conductivities in the same range.

SEM imaging of the Cu+CNT-based spin-coated layers (Fig. 9) above shows that there were some observable differences in layer morphology due to the amount of co-solvent. Inkjet-printed single-pixel line profile scans across the width of the line (Figure 12), however, reveal differences in morphologies more clearly, which suggests that solvent composition induced flows are present during drying. Outward convective flows appear dominant for composition [C], leading to particle migration towards the edges of the line, whereas a large enough counteracting Marangoni flow is likely induced in compositions [K] and [L], leading to a more even particle distribution along the width of the line.

The surface tension for all compositions is very similar (27.1 ± 0.3 mN/m), further suggesting that differences in line widths and particle distribution are arising from varying magnitudes of Marangoni flows during drying, and are not related to the initial fluid–substrate equilibrium contact angle.

SEM images taken from the center and edges of the printed lines do not reveal visible differences in morphology or particle packing, which would directly explain the conductivity differences, in contrast to the findings of Jeong et al.[15] and Kim et al.,[30] where a direct link between solvent composition, layer morphology, and conductivity of inkjet-deposited lines of a metallic nanoparticle fluid is shown. In[15] the layer resistivities of the inkjet-deposited patterns using an EG-containing copper fluid compared to the pattern printed using non-EG-containing fluid were 11 μΩ cm (9.1×10^6 S/m) and 38 Ω cm (2.6×10^6 S/m), respectively. This approximately 3.5-fold increase in conductivity is comparable to the 2.6-fold increase obtained when comparing compositions [C] and [L] of this study.

Jetting performance characterization for compositions [C], [K], and [L] shows that, as expected, an increase of the highest viscosity component (EGBE) provides more stable drop formation. Composition [L] allows for stable tail merge without satellite droplets at a higher velocity of 7 m/s compared to composition [C] at jetting frequencies up to 5 kHz. Also, an improvement in latency is observed with an increase of EGBE concentration.

SUMMARY AND CONCLUSIONS

The formulation of a conductive inkjettable fluid based on carbon-coated copper nanoparticles has been demonstrated. Reasonable dispersion stability and promising jetting performance has been obtained with the optimized fluid formulation. At present, the material is not envisioned to replace printable silver, gold, or novel copper fluids in applications requiring high conductivity. Rather, the conductivity levels achieved suggest that the fluid is applicable, for example, for antistatic coatings, resistors, and sensors. Notable attributes of the developed fluid are its low cost and ease of processing and handling. Conductivity in the 10^{-1}–10 S/m range (7–8 orders of magnitude lower than that of bulk copper) has been achieved by depositing a single layer and without high-temperature annealing. The best dispersion stability has been obtained by a polymeric dispersing agent with basic pigment affinic groups that interact with the acidic groups adsorbed on the carbon-coated copper nanoparticle surface. The highest conductivity was also obtained with this dispersing agent, presumably due to its unique polymeric backbone which decomposes more easily than those of the other two tested dispersing agents. Promising inkjetting performance of the electrically best-performing fluid composition suggests that further optimization of the fluid can yield a robust inkjet-printable fluid for industrial applications. Furthermore it has been observed that CNTs grown in situ on the particle surface during the particle production process increase the conductivity of the deposited layers. CNTs also seem to enhance the dispersion stability. Optimizing the ratio of high and low boiling point solvents has been observed to affect the conductivity, presumably through its effect on layer morphology during the drying process.

Further work is suggested in optimizing the carbon layer and CNT growth. Tailoring the organic components such that the interparticle distance is minimized could significantly increase the conductivity. A densification step[7] could also potentially increase the conductivity. When high conductivity comparable to that of metallic copper is required, a further processing step, for example laser sintering, could possibly be applied in order to remove the graphitic coating and organic components between the particles to enable direct copper-to-copper particle conductance.

It has been shown previously that, by modifying the graphitic coating of the particles, the material can exhibit similar sensitivity to temperature- and pressure-dependent conductivity as currently used commercial spinels.[31] For such an application the achieved conductivity of the printed layer is sufficient. Furthermore, as the fluid preparation process is transferrable to carbon-coated nanoparticles in general, substituting the copper core with other metal cores (with for example magnetic properties) opens up a range of potential applications for carbon-coated nanoparticles.

In situ carbon coating of copper nanoparticles provides an effective means of handling and processing of nanosized copper in air, enabling easy formulation of solution-processable fluids. Further work remains to be done in order to obtain highly conductive layers of the material, as the attainable conductivity at present seems to be determined by the layer of graphitic carbon encapsulating the copper particles.

ACKNOWLEDGMENTS

BYK-Chemie GmbH is acknowledged for kindly providing the dispersing agents used in this work and for the characterization and the description thereof. The work described in this article has received funding from the European Community's Seventh Framework Programme under grant agreement no 228559.

REFERENCES

[1] A. Kamyshny and J. Steinke, "Metal-based inkjet inks for printed electronics," The Open Appl. Phys. J. **4**, 19 (2011).

[2] S. Magdassi, M. Grouchko, and A. Kamyshny, "Copper nanoparticles for printed electronics: routes towards achieving oxidation stability," Materials **3**, 4626 (2010).

[3] B. Park, D. Kim, S. Jeong, J. Moon, and J. Kim, "Direct writing of copper conductive patterns by ink-jet printing," Thin Solid Films **515**, 7706 (2007).

[4] Y.-S. Goo, Y.-I. Lee, N. Kim, K.-J. Lee, B. Yoo, S.-J. Hong, J.-D. Kim, and Y.-H. Choa, "Ink-jet printing of Cu conductive ink on flexible substrate modified by oxygen plasma treatment," Surf. Coat. Technol. **205**, S369 (2010).

[5] S. Jeong, K. Woo, D. Kim, S. Lim, J.-S. Kim, H. Shin, Y. Xia, and J. Moon, "Controlling the thickness of the surface oxide layer on Cu nanoparticles for the fabrication of conductive structures by ink-jet printing," Adv. Funct. Mater. **18**, 679 (2008).

[6] H.-S. Kim, S. R. Dhage, D.-E. Shim, and H. T. Hahn, "Intense pulsed light sintering of copper nanoink for printed electronics," Appl. Phys. A **97**, 791 (2009).

[7] N. A. Luechinger, E. K. Athanassiou, and W. J. Stark, "Graphene-stabilized copper nanoparticles as an air-stable substitute for silver and gold in low-cost ink-jet printable electronics," Nanotechnology **19**, 445201 (2008).

[8] A. K. Schaper, H. Hou, A. Greiner, R. Schneider, and F. Phillipp, "Copper nanoparticles encapsulated in multi-shell carbon cages," Appl. Phys. A: Mater. Sci. Process. **78**, 73 (2004).

[9] S. Wang, X. Huang, Y. He, H. Huang, Y. Wu, and L. Hou, "Synthesis, growth mechanism and thermal stability of copper nanoparticles encapsulated by multi-layer graphene," Carbon **50**, 2119 (2012).

[10] ANSI ESD S541-2008 *For the Protection of Electrostatic Discharge Susceptible Items: Packaging Materials for ESD Sensitive Items* (ANSI, Washington D.C.), www.ansi.org.

[11] K. Gilleo, *Polymer Thick Film* (Van Nostrand Reinhold, New York, 1996), p. 140.

[12] R. D. Deegan, O. Bakajin, and T. F. Dupont, "Capillary flow as the cause of ring stains from dried liquid drops," Nature **389**, 827 (1997).

[13] R. D. Deegan, O. Bakajin, T. F. Dupont, G. Huber, S. R. Nagel, and T. A. Witten, "Contact line deposits in an evaporating drop," Phys. Rev. E **62**, 756 (2000).

[14] J. Park and J. Moon, "Control of colloidal particle deposit patterns within picoliter droplets ejected by ink-jet printing," Langmuir **22**, 3506 (2006).

[15] P. Jeong, H. C. Song, W. W. Lee, S. S. Lee, Y. Choi, W. Son, E. D. Kim, C. H. Paik, S. H. Oh, and B.-H. Ryu, "Stable aqueous based Cu nanoparticle ink for printing well-defined highly conductive features on a plastic substrate," Langmuir **27**, 3144 (2011).

[16] J. Forsman, U. Tapper, A. Auvinen, and J. Jokiniemi, "Production of cobalt and nickel particles by hydrogen reduction," J. Nanoparticle Res. **10**, 745 (2008).

[17] J. German-Heins, M. Flury, A. Auvinen, K. E. J. Lehtinen, J. Enriquez, J. K. Jokiniemi, and R. Zilliacus, "Vaporisation rates of CsOH and CsI in conditions simulating a severe nuclear accident," J. Aerosol Sci. **31**, 1029 (2000).

[18] W. Koch, H. Lödding, W. Mölter, and F. Munzinger, "Verdünnungsystemfür die Messung hochkonzenrieter Aerosole mit optischen Partikelzähler," Staub, Reinhaltung der Luft **48**, 341 (1988).

[19] E. O. Knutson and K. T. Whitby, "Aerosol classification by electric mobility: apparatus, theory, and applications," J. Aerosol Sci. **6**, 443 (1975).

[20] S. C. Wang and R. C. Flagan, "Scanning electrical mobility spectrometer," Aerosol Sci. Technol. **13**, 230 (1990).

[21] Y.-S. Cheng, "Instrumental techniques/Condensation detection and diffusion size separation techniques," *Aerosol Measurement — Principles, Techniques and Applications* (Van Nostrand Reinhold, New York, 1993), pp. 427–451.

[22] A. Kamyshny, M. Ben-Moshe, S. Aviezer, and S. Magdassi, "Ink-jet printing of metallic nanoparticles and microemulsions," Macromol. Rapid Commun. **26**, 281 (2005).

[23] B. Derby, "Inkjet printing of functional and structural materials: fluid property requirements, feature stability, and resolution," Ann. Rev. Mater. Res. **40**, 395 (2010).

[24] S. Magdassi, *The Chemistry of Inkjet Inks* (World Scientific, Singapore, 2010), p. 31.

[25] S. G. Yiantsios and B. G. Higgins, "Marangoni flows during drying of colloidal films," Phys. Fluids **18**, 082103 (2006).

[26] W. J. Hyun, S. H. Im, O. O. Park, and B. D. Chin, "Corrugated structure through a spin-coating process for enhanced light extraction from organic light-emitting diodes," Org. Electron. **13**, 579 (2012).

[27] Y. Kopelevich, R. R. da Silva, J. C. M. Pantoja, and A. M. Bratkovsky, "Negative c-axis magnetoresistance in graphite," Phys. Lett. A **374**, 4629 (2010).

[28] S. D. Hoath, I. M. Hutchings, G. D. Martin, T. R. Tuladhar, M. R. Mackley, and D. Vadillo, "Links between ink rheology, drop-on-demand jet formation, and printability," J. Imaging Sci. Technol. **53**, 041208-1–041208-8 (2009).

[29] H. Wijshoff, "The dynamics of the piezo inkjet printhead operation," Phys. Rep. **491**, 77 (2010).

[30] D. Kim, S. Jeong, B. K. Park, and J. Moon, "Direct writing of silver conductive patterns: Improvement of film morphology and conductance by controlling solvent compositions," Appl. Phys. Lett. **89**, 264101 (2006).

[31] E. K. Athanassiou, C. Mensing, and W. J. Stark, "Insulator coated metal nanoparticles with a core/shell geometry exhibit a temperature sensitivity similar to advanced spinels," Sensors Actuators A **138**, 120 (2007).